The benefit of brightness temperature assimilation for the SMAP Level-4 surface and root-zone soil moisture analysis over mainland China

Jianxiu Qiu[1,2], Jianzhi Dong[3], Wade T. Crow[3], Xiaohu Zhang[4,5], Rolf H. Reichle[6], Gabrielle J. M. De Lannoy[7]

[1]Guangdong Provincial Key Laboratory of Urbanization and Geo-simulation, School of Geography and Planning, Sun Yat-sen University, Guangzhou, 510275, China

[2]Southern Laboratory of Ocean Science and Engineering (Guangdong, Zhuhai), Zhuhai, 519000, China

[3]USDA ARS Hydrology and Remote Sensing Laboratory, Beltsville, MD 20705, USA

[4]National Engineering and Technology Center for Information Agriculture, Nanjing Agricultural University, Nanjing, China

[5]Jiangsu Key Laboratory for Information Agriculture, Nanjing Agricultural University, Nanjing, China

[6]Global Modeling and Assimilation Office, NASA Goddard Space Flight Center, Greenbelt, MD, USA

[7]Department of Earth and Environmental Sciences, KU Leuven, Heverlee, Belgium

Correspondence to: Jianxiu Qiu (qiujianxiu@mail.sysu.edu.cn)

16 **Abstract.** The Soil Moisture Active Passive (SMAP) Level-4 (L4) product provides global estimates of surface soil

17 moisture (SSM) and root-zone soil moisture (RZSM) via the assimilation of SMAP brightness temperature (Tb)

18 observations into the Catchment Land Surface Model (CLSM). Here, using in-situ measurements from 2474 sites in

19 mainland China, we evaluate the performance of soil moisture estimates from the L4 data assimilation (DA) system

20 and from a baseline "open-loop" (OL) simulation of CLSM without Tb assimilation. Using random forest regression,

21 the efficiency of the L4 DA system (i.e., the performance improvement in DA relative to OL) is attributed to eight

22 control factors related to the CLSM and as well as tau-omega radiative transfer model (RTM) components of the L4

23 system. Results show that the Spearman rank correlation (R) for L4 SSM with in-situ measurements increases for 77%

24 of the in-situ measurement locations (relative to that of OL), with an average R increase of approximately 14% ($\Delta R =$

25 0.056). RZSM skill is improved for about 74% of the in-situ measurement locations, but the average R increase for

26 RZSM is only 7% ($\Delta R = 0.034$). Results further show that the SSM DA skill improvement is most strongly related to

27 the difference between the RTM-simulated Tb and the SMAP Tb observation, followed by the error in precipitation

28 forcing and microwave soil roughness h. For the RZSM DA skill improvement, these three dominant control factors

29 remain the same, although the importance of soil roughness exceeds that of the Tb simulation error, as the soil

30 roughness strongly affects the ingestion of DA increments and further propagation to the subsurface. For the skill of

31 the L4 and OL estimates themselves, the top two control factors are the precipitation error and the SSM-RZSM

32 coupling strength error, both of which are related to the CLSM component of the L4 system. Finally, we find that the

33 L4 system can effectively filter out errors in precipitation. Therefore, future development of the L4 system should

34 focus on improving the characterization of the SSM-RZSM coupling strength.

35

36 **Keywords.** SMAP Level 4, soil moisture, data assimilation, attribute analysis, random forest regression

37 **1 Introduction**

38 Soil moisture modulates water and energy feedback between the land surface and the lower atmosphere by determining

39 the partitioning of incoming net radiation into latent and sensible heat (Seneviratne et al., 2010, 2013). High-quality,

40 global-scale soil moisture products have become increasingly available in recent years. In particular, the L-band NASA

41 Soil Moisture Active Passive (SMAP) satellite mission (Entekhabi et al., 2010; Piepmeier et al., 2017) has significantly

42 improved the skill of available, global-scale soil moisture products. However, the SMAP observations contain temporal

43 data gaps and are only representative of conditions within only the first 5 cm of the vertical soil moisture column

44 (Entekhabi et al., 2010). To address these limitations, the SMAP Level-4 Surface and Root-Zone Soil Moisture (L4)

45 algorithm assimilates SMAP brightness temperature (Tb) observations into the NASA Catchment Land Surface Model

46 (CLSM) to derive an analysis of surface (0–5 cm) and root-zone (0–100 cm) soil moisture estimates with global, 3-

47 hourly coverage (Reichle et al., 2017a; Reichle et al., 2017b; Reichle et al., 2019).

48 However, the performance of a land data assimilation (DA) system is sensitive to the DA parameterization and requires

49 careful assessment. For instance, Reichle et al. (2008) demonstrate that DA based on incorrect assumptions of modeling

50 errors and observation errors can degrade soil moisture estimates, compared with the case of not performing DA, which

51 is commonly referred to as the "open-loop" (OL) baseline. Theoretically, the optimality of DA can be evaluated using

52   so-called "innovations", or observation-minus-forecast residuals; however, an investigation of the innovations alone

53   is often insufficient to determine if the soil moisture analysis is optimal, as the innovations are affected by multiple

54   factors (Crow and Van Loon, 2006).

55   Recently, Dong et al. (2019a) proposed a novel statistical framework for evaluating the performance of a soil moisture

56   DA system. Specifically, they demonstrated that the relative skill of surface soil moisture (SSM) estimates acquired

57   with and without DA can be estimated using the ratio of their correlations with just one noisy but independent ancillary

58   remote sensing product. This approach was applied to the SMAP L4 system using Advanced Scatterometer soil

59   moisture retrievals. Their results show that the benefit of SMAP DA is closely related to densities of both rain gauge

60   and vegetation. Generally, higher rain gauge density indicates lower error in precipitation forcing, and lower vegetation

61   density indicates higher background model performance - both conditions lead to reduced SMAP DA benefit. However,

62   due to the limited availability of independent root-zone soil moisture (RZSM) products for performing statistical error

63   estimation, this method is only applicable for SSM estimates.

64   Relative to SSM, the efficiency of assimilating land surface observations to improve RZSM is complicated by model

65   structural error that affects the ability of the DA to update unobserved model states. For instance, Kumar et al. (2009)

66   identified the surface–root zone coupling strength, which is the result of a model-dependent representation of processes

67   related to the partitioning of rainfall into infiltration, runoff, and evaporation components, as an important factor for

68   determining RZSM improvement associated with the assimilation of SSM retrievals. Their synthetic experiments

69   suggest that, faced with unknown true subsurface physics, overestimating the surface–root zone coupling in the land

70   model is a more robust strategy for obtaining skill improvements in the root zone than under-estimating the coupling.

71   Likewise, Chen et al. (2011) suggested that the Soil and Water Assessment Tool significantly under-predicts the

72   magnitude of vertical soil water coupling in the Cobb Creek Watershed in southwestern Oklahoma, USA, and this lack

73   of coupling impedes the ability of DA to effectively update soil moisture in deep layers, groundwater flow and surface

74   runoff. In the context of the present paper, the evaluation of L4 RZSM estimates has been limited to SMAP core

75   validation and sparse network sites (Reichle et al., 2017a; Reichle et al., 2017b; Reichle et al., 2019). With such limited

76   validation sites, the RZSM skill of the L4 product at the global scale remains uncertain.

77   The primary objective of this study is to assess the DA skill improvement, i.e., the performance improvement in DA

78   results relative to the OL baseline of the L4 product, and to further determine how DA skill improvement varies as a

79   function of the major aspects in the system. As mentioned above, the modeling portion of the L4 system consists of

80   two components: land surface modelling (LSM) and radiative transfer modelling (RTM). Therefore, we select control

81   factors from each of the two components. For the LSM component, the errors can be attributed to potential factors

82   including: 1) model input forcing errors of a) precipitation and b) LAI; 2) model structure errors in a) characterizing

83   SSM-RZSM coupling strength and b) the presence of vertical variability in soil properties; 3) model output error of

84   LE. For the RTM component, errors are characterized by: 1) DA innovation, i.e., SMAP-observed minus RTM-

85   simulated Tb; 2) the environmental factors that complicate the DA analysis when assimilating Tb observations, which

86   include the magnitude of a) microwave soil roughness and b) LAI. These eight control factors from the above-

87   mentioned five aspects determine the crucial aspects of both the LSM and RTM components in the L4 system and are

88   readily quantifiable using remote sensing products. Thus, they are selected to investigate the mechanism underlying

89   the L4 improvement observed in this study.

90   Therefore, to achieve the two major objectives, we first evaluate the performance of L4 SSM and RZSM estimates

91   using 2474 sites in mainland China with soil moisture profile measurements (generally acquired at sub-surface depths

92   between 10 and 50 cm) during the two-year period of 2017 to 2018. Next, the in-situ measurements are used to assess

93   the DA skill improvement of the L4 system, which is defined as the skill difference between the L4 estimates and the

94   OL baseline. Additionally, we apply a machine-learning technique to quantify by how much the eight potential control

95   factors drive the spatial variations in the efficiency of the L4 system. In this way, we seek to prioritize future

96   enhancements to the L4 system.

97   **2 Data and Methods**

98   In this section, we briefly describe the SMAP L4 soil moisture product (Section 2.1), the network of in-situ soil

99   moisture observations in mainland China (Section 2.2), the above-mentioned control factors and ancillary data sources

100   (Section 2.3), and the vertical coupling metric used in the skill assessment (Section 2.4). Next, we introduce the double

101   instrumental variable (IVd) method employed to determine the errors in control factors that cannot be determined using

102   ground observations (Section 2.5). Finally, we describe the random forest (RF) regression method used to identify the

103   main factor(s) (out of the eight control factors from both CLSM and RTM aspects) that affect the spatial variations in

104   SMAP L4 DA skill improvement and L4 performance (Section 2.6).

105   **2.1 SMAP L4 soil moisture product**

106   The SMAP L4 soil moisture product (version 4; Reichle et al., 2019) is generated by assimilating the SMAP L1C

107   Radiometer half-orbit 36 km Equal-Area Scalable Earth (EASE) Grid Tb observations (Version 4 SPL1CTB; Chan et

108   al., 2016) into the CLSM. The SMAP Tb observations are assimilated at 3-h intervals using a spatially distributed, 24-

109   member ensemble Kalman filter (Reichle et al. 2017b). The surface meteorological forcing data are from the global

110   Goddard Earth Observing System (GEOS) Forward Processing atmospheric analysis (Lucchesi, 2013), with

111   precipitation corrected using the daily, 0.5-degree, gauge-based Climate Prediction Center Unified (CPCU) product

112   (Xie et al. 2007). The L4 product provides global, 9-km, 3-hourly surface (0–5 cm) and root-zone (0–100 cm) soil

113   moisture estimates along with related land surface fields and analysis diagnostics. For the present study, we aggregate

114   all soil moisture estimates to daily averaged (00:00 to 23:59 UTC) data. The OL baseline is a model-only, ensemble

115   CLSM simulation without the assimilation of SMAP Tb observations but otherwise using the same configuration,

116   including perturbations, as in the L4 system (Reichle et al., 2020).

117   The SMAP L4 assimilation system includes a zero-order "tau-omega" forward RTM (De Lannoy et al., 2013) that

118   converts SSM and surface soil temperature into L-band brightness temperature estimates. Select parameters of the L4

119   RTM, including the: microwave soil roughness parameter h, vegetation structure parameter τ, and the microwave

120   scattering albedo ω, are calibrated using multi-angular L-band brightness temperature observations from the Soil

121   Moisture Ocean Salinity (SMOS) mission (De Lannoy et al., 2014). The L4 RTM parameterizes microwave soil

122   roughness as a function of SSM (De Lannoy et al., 2013, their equation B1). Here, we use this parameterization to

123   compute the 2017-2018 daily averaged microwave soil roughness estimates as one potential indicator of DA skill

124   improvement (Section 2.3).   The necessary parameters are obtained from L4 "Land-Model-Constants" output

125   Collection (last access: 8 July 2020; DOI: https://doi.org/10.5067/KGLC3UH4TMAQ; Reichle et al., 2018a). The L4

126   "Analysis-Update-Data" output Collection includes RTM predictions of Tb and the assimilated SMAP Tb observations

127   (last access: 8 July 2020; DOI: https://doi.org/10.5067/60HB8VIP2T8W; Reichle et al., 2018b).

128   To avoid the impact of seasonality, we perform our analysis using anomaly time series, derived by subtracting a

129   seasonally varying (daily) climatology from each raw time series. The climatology of a given time series is obtained

130   by sampling the mean value of all soil moisture estimates that fall within a 31-day moving window centered on a

131   particular day-of-year. Moreover, L4 estimates of land latent heat flux (LE), land sensible heat flux (SH) and the

132   climatological LAI inputs to CLSM and the RTM, are obtained from the L4 "Geophysical-Data" output Collection

133   (last access: 6 April 2020; DOI: https://doi.org/10.5067/KPJNN2GI1DQR; Reichle et al., 2018c). These datasets are

134   also used to compute control factors to explain spatial variations in the DA skill improvement of the L4 system (Section

135   2.3).

136   **2.2 Soil moisture validation data**

137   In-situ soil moisture measurements during 2017 and 2018 are collected from a national network of Chinese Automatic

138   Soil Moisture Observation Stations (CASMOS) maintained by the Chinese Meteorological Administration (CMA;

139   Han et al., 2017). In total, soil moisture measurements from 2474 separate stations array across mainland China, and

140   covering different land use types, are collected. At each CASMOS site, frequency domain reflectometry-based

141   instruments (DNZ1, DNZ2, and DNZ3) are used to record hourly volumetric soil moisture content within the following

142   vertical depth ranges: 0–10, 10–20, 20–30, 30–40, and 40–50 cm below the surface. These hourly estimates (at multiple

143   depths) are then aggregated into daily values and linearly averaged (vertically) to produce 0-10 cm (SSM) and 0-50

144   cm (RZSM) in situ soil moisture measurements – which are subsequently used to validate the L4 and OL SSM (0-5

145   cm) and RZSM (0-100 cm) estimates. Note that Spearman correlation rather than Pearson correlation is used for L4

146   and OL validation because Pearson correlation assumes linear consistency of the underlying variables and is more

147   sensitive to outliers. By employing Spearman's rank correlation, we avoid introducing ad-hoc thresholds and do not

148   exclude soil moisture outliers. Nonetheless, we repeat the analysis based on Pearson correlation (not shown) and find

149   that the results are qualitatively consistent with the results using Spearman's correlation.

150   Ground observations within the same 9-km EASE grid were averaged for comparisons against the collocated 9-km L4

151   and OL soil moisture estimates. A total of 2287 individual 9-km EASE grid cells within mainland China are included

152   in the analysis. Among them, 92.35% of grid cells contain one in-situ site, 7.26% contain two sites, 7 grid cells contain

153   three sites, and the remaining two grid cells contain four and five sites respectively. Figure 1 shows the number of in-

154   situ CASMOS sites within each 9-km EASE grid.

155
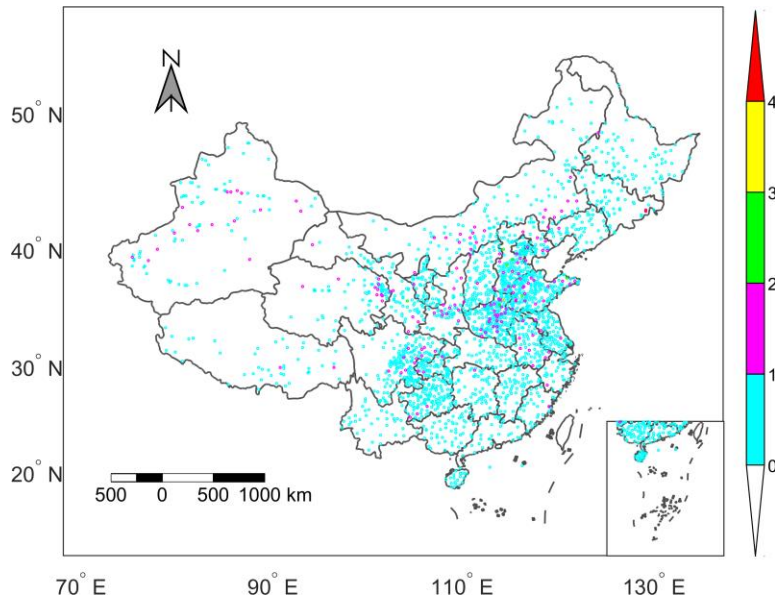
Figure 1: The number of in-situ CASMOS sites within each 9-km EASE grid across mainland China.

156

157

2.3 Explanatory data products

158

159 As discussed above, our hypothesis is that the efficiency of the SMAP L4 system will be sensitive to the ability of the

160 ensemble-based L4 analysis in filtering errors that exist in CLSM, the RTM forecast Tb, and the assimilated SMAP

161 Tb observations. We therefore consider two separate categories of factors that potentially control spatial variations in

162 DA skill improvement. The factors are summarized in Table 1.

163 The first category represents a range of factors known to affect the skill of soil moisture estimates derived from the

164 LSM (in this case, CLSM). The five control factors in this category are: 1) the error in precipitation forcing, 2) the

165 error in (input) LAI, 3) the error in (output) LE, 4) the magnitude of mean error in CLSM SSM-RZSM coupling

166 strength, and 5) the presence of vertical variability in soil properties (defined as the difference in clay fraction across

167 the vertical soil profile). Note that such variability represents a potential source of error because, with the exception of

168 some surface-layer moisture transport parameters, CLSM assumes soil texture and associated soil parameters are

169 vertically homogeneous within the soil column. However, the Harmonized World Soil Database (HWSD) often

170 captures distinct vertical variations in soil properties. Therefore, since it is largely neglected by CLSM, the magnitude

171 of vertical heterogeneity in soil texture may be an effective proxy for overall CLSM soil moisture accuracy. In addition,

172 note that since LH and SH are generally (strongly) anti-correlated, it is not appropriate to include both in a single

173 random forest analysis – since including both would yield biased (high) regression weights for LH and SH.

174 The second category contains three factors that affect radiative transfer modeling (RTM) and therefore DA updates.

175 These include: 1) estimates of the DA innovation, namely difference between SMAP Tb observations and RTM Tb

176 simulations, 2) the magnitude of microwave soil roughness, and 3) the magnitude of LAI (as a proxy for the vegetation

177 optical depth at microwave frequencies, which modulates the contribution of surface soil to the observed Tb).

6

178 The control factors take a variety of forms. Some factors are based on estimates of the errors fed into the L4 system,

179 namely: 1) the error in CLSM rainfall forcing data; 2) error in SSM-RZSM coupling strength; 3) vertical variability of

180 clay fraction; 4) SMAP L4 LAI error; 5) output LE error; 6) Tb error. Other factors consist of the magnitude of the

181 variable itself, namely the magnitude of microwave soil roughness and annual mean LAI. Note that LAI is used in

182 both ways: LAI error is used to predict OL performance (because LAI is an important input into CLSM), while mean

183 LAI is used to explain DA performance (because increased LAI is associated with decreased soil moisture information

184 in microwave observations).

185 Note that the LAI used in the L4 system is a merged climatology from Moderate Resolution Imaging Spectroradiometer

186 (MODIS) and Geoland data based on satellite observations of the Normalized Difference Vegetation Index (Mahanama

187 et al., 2015; Reichle et al., 2017a). Therefore, to indicate the magnitude by which the LAI of each grid cell typically

188 deviates from its long-term climatology, we use the temporal standard deviation for the anomaly time series of a

189 benchmark LAI time series as a measure of the error in the LAI value used in the L4 system. This benchmark LAI is

190 from the SPOT-Vegetation (SPOT VGT) product and includes inter-annual variations (Section 2.3.3). Owing to the

191 lack of reference Tb observations at similar satellite overpass times and locations, Tb errors are gauged using the time

192 series standard deviation of the observation-minus-forecast (O-F) Tb residuals, which indicate the typical misfit

193 between the model forecast Tb and the rescaled SMAP Tb observations. This rescaling process ensures zero-mean

194 differences between Tb observations and forecasts and involves a seasonal multiyear-mean bias correction, which

195 makes sure that the DA only corrects for errors in short-term and inter-annual variations and not for errors in the

196 climatological seasonal cycles of the modeled soil moisture or other land surface fields. The standard deviation of the

197 O-F Tb residuals measures the total error in Tb observation space.

198 The exact data sets and the metrics utilized for evaluating all eight control factors are summarized in Table 1.

Table 1 Benchmark data sets and metrics used for evaluating control factors of SMAP L4

Factor category	Control factor	Dataset/Benchmark	Temporal resolution	Spatial resolution	Data range	Metrics
LSM	Precipitation error	Rain gauge (CGDPA)	daily	0.25 °	2017-2018	Spearman's rank correlation R
	SSM-RZSM coupling strength error	CASMOS	daily	NA	2017-2018	ΔCP (see Section 2.4)
	Vertical variability of clay fraction	HWSD	NA	9 km	NA	Difference in clay fraction between topsoil (0-30 cm) and root-zone (0-100 cm) layers
	SMAP L4 LAI error	SPOT-VGT LAI	10 d	1 km	2017-2018	Temporal standard deviation of SPOT VGT LAI anomaly
	LE error	FLUXCOM	daily	(1/120) °	2017-2018	IVd-based R
RTM	Tb error	SMAP L4	daily	9 km	2017-2018	Temporal standard deviation of O-F Tb residuals
	Microwave soil roughness	SMAP L4	daily	9 km	2017-2018	Temporal average based on De Lannoy et al. (2013)
	Annual mean LAI	MODIS/Geoland-based product	daily	9 km	2017-2018	Climatological mean

201 **2.3.1 Gauge-based precipitation gridded product**

202 Errors in the precipitation data used to force the CLSM within the SMAP L4 system are estimated via Spearman's

203 rank correlation with available rain-gauge observations. These network observations are based on an analysis of ~2400

204 rain gauge stations distributed across mainland China (Shen et al., 2015). Recently, the China Gauge-based Daily

205 Precipitation Analysis (CGDPA) with a spatial resolution of 0.25 °×0.25 °based on this network was constructed and

206 has been made operational over mainland China (last access: 28 April 2020;

207 http://data.cma.cn/data/cdcdetail/dataCode/SEVP_CLI_CHN_PRE_DAY_GRID_0.25.html). CGDPA uses a

208 modified version of climatology-based optimal interpolation (OI) with topographic correction proposed by Xie et al.

209 (2007). In this process, the daily precipitation climatology over mainland China is optimized and rebuilt using the 30-

210 year average precipitation observations from ~2400 gauges of the period 1971–2000 (Shen et al., 2010). CGDPA is

211 shown to have smaller bias and root mean square error (for instance, 13.51 mm day^{-1} vs. 17.02 mm day^{-1} for

212 precipitation of 25.0–50.0 mm day^{-1}) than the CPCU product used in the SMAP L4 system, which is based on fewer

213 than 400 gauge sites over mainland China (Shen et al., 2015).

214 **2.3.2 FLUXCOM LE estimates**

215 The FLUXCOM ensemble of global land-atmosphere energy fluxes is used to evaluate error in L4 LE estimates. This

216 ensemble merges energy flux measurements from FLUXNET eddy covariance towers with remote sensing and

217 meteorological data based on four broad categories of machine learning method (namely tree-based methods,

218 regression splines, neural networks, and kernel methods) to estimate global gridded net radiation, latent and sensible

219 heat and their related uncertainties (Jung et al., 2019). The resulting FLUXCOM database has a 0.0833 ° spatial

220 resolution when applied using MODIS remote sensing data. The monthly energy flux data of all ensemble members,

221 as well as the ensemble estimates from the FLUXCOM initiative, are freely available (CC4.0 BY license) from the

222 Data Portal (http://fluxcom.org/), while the daily- and 8-day FLUXCOM products are available upon request from

223 dataset provider Martin Jung (last access: 14 April 2020). To calculate the LE error, we collected the daily, high spatial

224 resolution FLUXCOM product and extracted the LE estimates where in-situ soil moisture sites are located.

225 **2.3.3 SPOT VGT LAI**

226 The data set used as a benchmark for assessing leaf area index (LAI) errors present in the SMAP L4 analysis is derived

227 from the SPOT/VEGETATION and PROBA-V LAI products (version 2) that generated every 10 days (at best) with a

228 spatial resolution of 1 km. The SPOT LAI version 2 product GEOV2 is provided by the Copernicus Global Land

229 Service (last access: 15 April 2020; https://land.copernicus.eu/global/products/LAI; Baret et al., 2013). It capitalizes

230 on the development of already existing products: CYCLOPES version 3.1 and MODIS collection 5 based on neural

231 networks (Baret et al., 2013; Verger et al., 2008). Compared to version 1, the version 2 products are derived from top

232 of canopy daily reflectances, which ensures reduced sensitivity to missing observations and avoids the need for a

233 bidirectional reflectance distribution function model.

234 **2.3.4 HWSD soil texture**

235 The soil texture information is from the HWSD attribute database (v1.2; FAO/IIASA/ISRIC/ISSCAS/JRC, 2012),

236 which is a 30 arc-second raster database with 15773 different soil-mapping units worldwide. It provides information

237 on the standardized soil parameters for topsoil (0–30cm) and subsoil (30-100 cm) separately. In this study, we use the

238 difference of clay fractions between topsoil (0-30cm) and the aggregated 0-100cm layer to measure the vertical clay

239 fraction variation at each 9-km grid cell.

2.4 Vertical coupling metric

241 The RZSM time series generally show decreased temporal dynamics relative to SSM. As a result, overestimated SSM-

242 RZSM coupling tends to spuriously increase the (correlation-based) similarity of SSM and RZSM time series, and

243 thereby, overestimate RZSM temporal variability. Therefore, analogous to Kling-Gupta efficiency (Gupta et al., 2009),

244 we define the SSM-RZSM coupling strength (CP) as:

$$CP = 1 - \sqrt{(R\text{-}1)^2 + (\alpha\text{-}1)^2} \qquad (1)$$

245 where R is the Spearman's rank correlation between SSM and RZSM, and α is the ratio of temporal standard deviation

246 of SSM to that of RZSM. The CP estimation is based on anomaly time series of both SSM and RZSM. A CP value of

247 one represents the extreme case where RZSM is identical to SSM, i.e., a strongly coupled case. Likewise, a CP of zero

248 represents the opposing case of completely uncoupled time series. Cases with negative CP do not exist in this study.

249 Observed CP (CP_{obs}) was based on comparisons between 0-10 cm "surface" and 0-50 cm "root-zone" in-situ

250 observations and used as a benchmark. In contrast, CP estimates of OL (CP_{OL}) was based on the comparison of 0-5 cm

251 "surface" and 0-100 cm "root-zone" estimates. Therefore, the surface versus root-zone storage contrast in the

252 observation time series is less than that of the L4 estimates. This will likely cause the observed correlation between

253 surface and root-zone time series to be systematically higher than the analogous vertical correlation calculation for L4

254 estimates. However, this bias is partially corrected for by the second term in Eq. (1) – since the observed α ratio will,

255 by the same token, tend to be smaller (i.e. closer to one) than α sampled from the L4 analysis. Such ability to

256 compensate for vertical depth differences is a key reason we apply CP, rather than *simple correlation*, as a vertical

257 coupling strength metric. Nevertheless, it should be noted that our main interest here lies in describing spatial variations

258 in (CP_{OL} - CP_{obs}) and care should be taken when interpreting raw (CP_{OL} - CP_{obs}) differences as an *absolute* measure of

259 L4 vertical coupling bias.

2.5 Double instrumental variable (IVd) method

261 The benchmark data set of FLUXCOM LE described above contains error that is assumed to be of a similar order of

262 magnitude as the L4 LE dataset it is applied to evaluate. Therefore, in an attempt to correct for the impact of this error,

263 the LE error used here as a control factor is obtained via a double instrumental variable (IVd; Dong et al., 2019b)

264 analysis approach that minimizes the spurious impact of random errors in benchmark data sets. As shown in Dong et

265 al. (2019b), for the evaluation of two time series containing autocorrelated errors, IVd is more robust than a single

266 instrumental variable based algorithm, therefore we apply IVd to evaluate the LE error.

267   IVd is a modified version of triple collocation (TC) analysis. In TC analysis (McColl et al., 2014), geophysical
268   variables obtained from three independent sources (x_t, y_t and z_t) at time t are assumed to be linearly related to the true
269   signal P_t as:

$$x_t = \alpha_x P_t + B_x + \varepsilon_{x,t} \tag{2}$$

270   where the α_x is a scaling factor; B_x is a temporal constant bias and $\varepsilon_{x,t}$ is zero-mean random error.
271   As opposed to the TC method, IVd uses only two independent products (x, y) to characterize geophysical data product
272   errors. This method introduces two instrumental variables I, which is the lag-1 time series of x, and J, which is the lag-
273   1 time series of y, respectively.

$$I_t = \alpha_x P_{t-1} + B_x + \varepsilon_{x,t-1} \tag{3}$$

$$J_t = \alpha_y P_{t-1} + B_y + \varepsilon_{y,t-1} \tag{4}$$

274   Therefore, assuming that the errors of two independent products are serially white, the covariance between instrumental
275   variables and products can be written as follows:

$$C_{Ix} = \alpha_x^2 L_{PP} \tag{5}$$

$$C_{Jy} = \alpha_y^2 L_{PP} \tag{6}$$

276   where C represents the covariance of the subscript products. For instance, C_{Ix} represents the covariance of x and its
277   instrumental variable I. Variable L_{PP} is the lag-1 auto-covariance of the true signal. Combining Eqs. (5) and (6), the
278   scaling ratio s_{ivd} of the two products x and y can be written as:

$$s_{ivd} = \sqrt{\frac{C_{Ix}}{C_{Jy}}} \tag{7}$$

279   Based on Eq. (7), their correlation with truth can be estimated as:

$$R_{Px}^2 = \frac{C_{xy} s_{ivd}}{C_{xx}} \tag{8}$$

11

$$R_{Py}^2 = \frac{C_{xy}}{C_{yy}s_{ivd}}$$
(9)

280   In this way, the error in the L4 LE (measured by IVd-based correlation with truth) can be estimated robustly using the

281   FLUXCOM LE product described in Section 2.3.2.

282   **2.6 Random forest regression**

283   A random forest (RF) regression approach is used to rank and quantify the importance of the eight control factors

284   introduced above (Table 1) for describing spatial patterns in DA skill improvement for both SSM and RZSM estimates.

285   The RF method is a supervised learning algorithm based on an averaged ensemble of decision trees (Breiman, 2001).

286   Unlike linear regression approaches, RF can capture non-linear interactions between the features and the target. In

287   addition, the normalization (or scaling) of data is not necessary in RF application. Another advantage of the RF

288   algorithm is that it can readily measure the relative importance of each feature on the estimates, which makes it highly

289   suitable for an attribution analysis. Therefore, based on the output of RF, key control factors determining the skill

290   improvement of SMAP DA are evaluated and ranked. The RF estimates are based on a 10-fold cross-validation

291   approach.

292   **3 Results**

293   **3.1 Validation of SMAP L4 and OL estimates of SSM and RZSM anomalies**

294   Figure 2 maps validation results (i.e., anomaly Spearman's rank correlation with in-situ observations, R) for SMAP L4

295   and associated OL soil moisture estimates. The skill patterns for OL and L4 are, in general, quite spatially consistent.

296   Both are characterized by an increasing trend of SSM estimation skill moving from northwest to southeast China (Fig.

297   2a and 2b) that matches the increasing density of the rain gauge network. In relative terms, the L4 product surpasses

298   the baseline OL's SSM skill for 77% of the 2287 9-km EASE grid cells containing ground observations – with a mean

299   R increase of $\Delta R = 0.056$ [-] and mean relative improvement versus R_{OL} of 14%.

300   Similar spatial patterns are observed for RZSM skill. As with SSM, generally higher consistency with in-situ RZSM

301   measurements is found in southeast China relative to northern and northwestern China. However, relative to SSM, the

302   benefit of SMAP data assimilation (i.e., L4) is reduced for RZSM and the mean relative R improvement is only 7%

303   ($\Delta R = 0.034$ [-]) (compare Fig. 2e and 2f). This reduction is expected since assimilated SMAP Tbs are primarily

304   sensitive to soil moisture conditions in the surface (0-5 cm) layer.
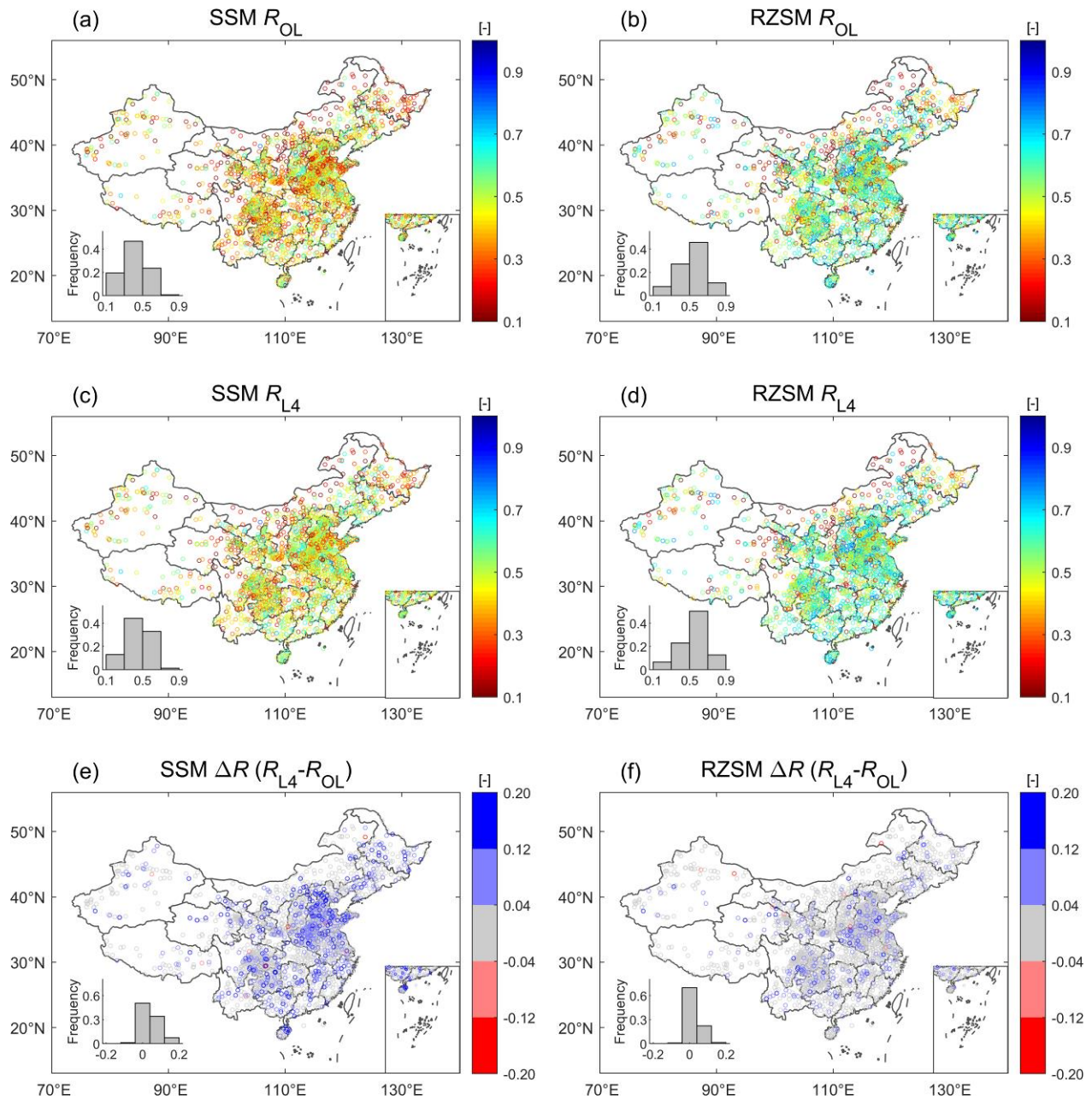
Figure 2: OL (a, b) and L4 (c, d) skills (*R* values) for SSM (left column) and RZSM (right column). DA skill improvement ($\Delta R = R_{L4} - R_{OL}$) for (e) SSM and (f) RZSM. Blue (red) colors in (e) and (f) indicate grid cells where L4 estimates are better (worse) than OL. Non-significant differences (based on a 1000-member bootstrapping analysis) are shaded grey. The lower left inset in each subplot indicates the frequency of binned *R*-values across all 9-km EASE grid cells containing ground observations.

3.2 Spatial distribution of potential factors controlling SMAP L4 DA performance

As described in Section 2.3, we select eight control factors that potentially influence the skill of SMAP L4 soil moisture estimates. Using the attribution analysis described in Section 2.6, these factors are used to explain the spatial variations

13

315   in skill and DA skill improvement seen in Fig. 2. As a first step, this section examines the spatial patterns inherent in
316   the eight control factors. Errors in the CLSM precipitation forcing are relatively higher in northern and northwestern
317   areas of China (Fig. 3a), where the gauge density is generally sparser than in southern China. Among the factors
318   representing CLSM structural errors, a pre-dominantly negative bias is observed in SSM-RZSM coupling strength
319   generally across China (i.e., lower CP_{OL} compared to CP_{obs}), while a very small number of grid cells show a positive
320   coupling strength bias in eastern China (dark green dots in Fig. 3b). This is expected since the coupling strength
321   generally decreases with coarser resolution, i.e., the vertical coupling strength of model is assumed much lower than
322   that of any single site. In addition, this may be partially attributed to layer depth differences, since CLSM represents
323   surface and root-zone depths of 0-5 cm and 0-100 cm, respectively, whereas the corresponding in-situ observations
324   represent the 0-10 cm and 0-50 cm layers. Therefore, CP_{OL} is likely to be systematically smaller than CP_{obs}. In addition,
325   the vertical variability of the clay fraction seems to show little spatial variation across mainland China (Fig. 3c). With
326   respect to CLSM LAI error, regions in southern China that have generally higher LAI show larger standard deviations
327   in SPOT LAI time series (Fig. 3d and 3h). The IVd-based estimates of SMAP L4 LE error, which represent a potential
328   control factor for water-balance errors in CLSM, generally show a low level of error across mainland China (Fig. 3e).
329   For O-F Tb residuals describing RTM-related error, a higher standard deviation of O-F Tb residuals is observed in the
330   North China Plain (Fig. 3f), which is very consistent in spatial distribution with areas displaying the highest and most
331   significant SSM prediction improvement (Fig. 2c). This is expected, as mentioned above, because O-F Tb residuals
332   are the basis for the soil moisture corrections (or increments) that are applied in the DA system as part of the L4
333   analysis. The 2017-2018 mean of soil roughness shows a relatively scattered spatial pattern (Fig. 3g), while the 2017-
334   2018 mean LAI shows higher values in southwest and southeast China (Fig. 3h).
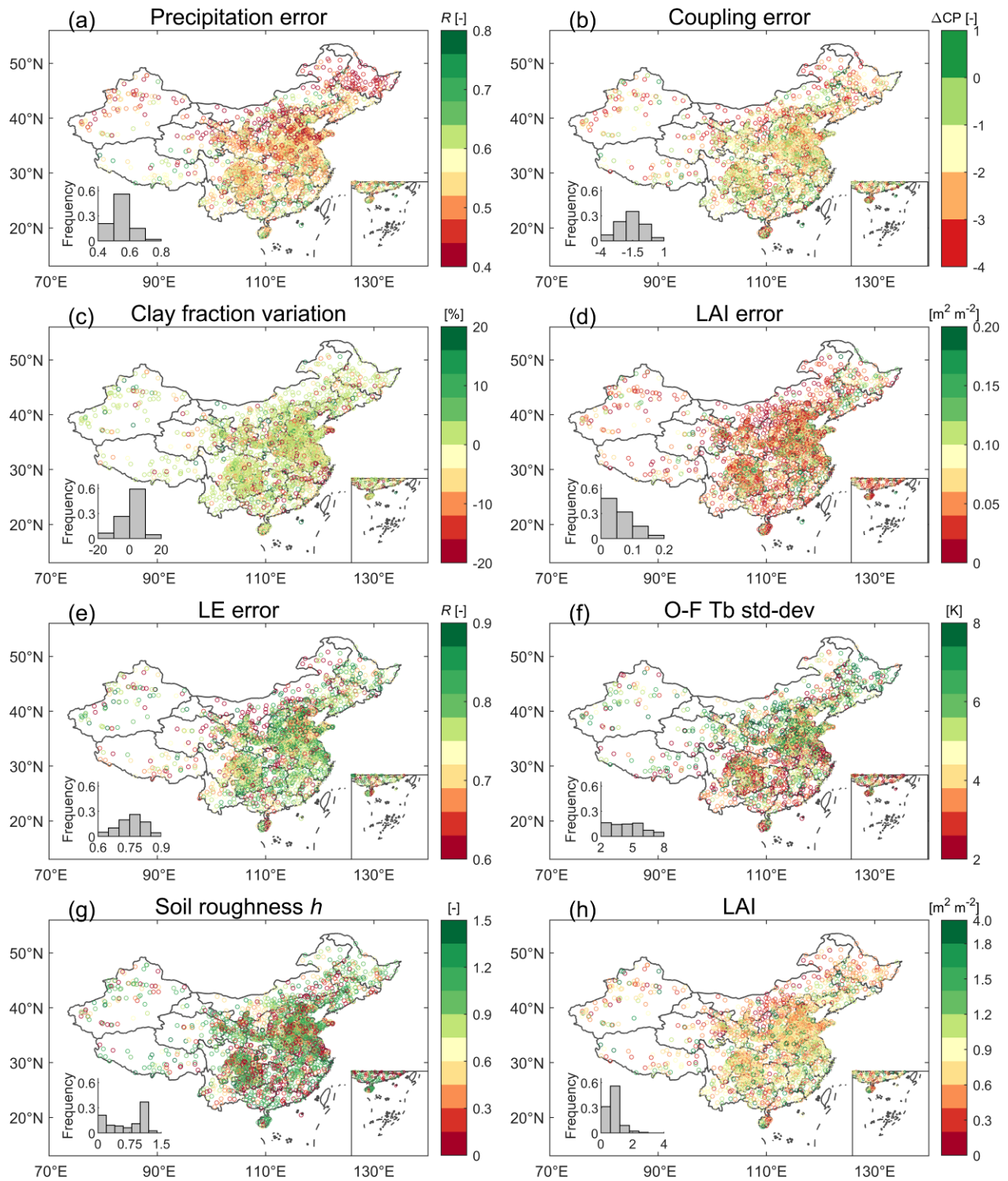
336 **Figure 3: Factors potentially influencing SMAP L4 performance over mainland China: (a) CLSM precipitation error**
337 **measured by the Spearman's rank correlation between CLSM precipitation and ground observations; (b) SSM-RZSM**
338 **coupling strength error (CP_{OL} minus CP_{obs}); (c) clay fraction variation (difference) across the soil profile; (d) error in LAI**
339 **input to L4; (e) IVd-based error of LE from L4; (f) O-F Tb standard deviation; (g) L4 microwave soil roughness; (h)**
340 **climatology mean of LAI input to L4. The last row shows factors that consist of the magnitude of the variable itself, while**
341 **the other rows show factors based on estimates of the errors that are fed into the L4 system.**

342

3.3 Attribution of SMAP L4 versus OL performance to control factors

3.3.1 Attribution using random forest regression

As mentioned above, RF regression is used to identify the relative importance of our eight control factors for determining the improvement of SMAP L4 DA (i.e., $\Delta R = R_{L4} - R_{OL}$) and also R_{L4} and R_{OL}. We first investigate the robustness of RF for predicting ΔR. To estimate the magnitude of randomness in the RF algorithm, we use 50 bootstrap runs. As shown in Fig. 4a, the 10-fold cross-validation test (228 validation samples) shows that the predicted and in-situ-based ΔR have a mean correlation of 0.72 and 0.46 for SSM and RZSM, respectively. In Fig. 4a, the mean and median of the cross-validation correlation are shown in black circle and black line respectively within the boxes, while the second and third quartiles of the cross-validation correlation are shown as the edges of boxes.

Given the sampling errors of ΔR, which is based on a two-year validation period, and the relatively low spatial variability in RZSM skill (Figs. 2f), the performance of RF is acceptable. In addition, ground-measurement upscaling error is likely a significant contributor to unexplainable spatial variability for ΔR in Fig. 2. In fact, Chen et al. (2016) found large spatial variability in the ability of point-scale SSM ground observations to describe grid cell-scale SSM dynamics. In-situ observations sites associated with larger random point-to-grid upscaling errors will introduce a spurious low bias into sampled estimates of ΔR values (see Appendix B in Dong et al., 2020). Therefore, part of the ΔR spatial variability observed in Fig. 2 is unrelated to any aspect of the L4 system and, therefore, unexplainable via our eight selected control factors.

Independent representativeness errors have an equal impact on both the L4 and OL skill assessments and should therefore not bias the relative skill assessments of L4 versus OL, particularly when these assessments are based on averaging across multiple grid cells. This holds if the location of ground-based measurements sites (within a footprint) is purely random. For the systematic sampling errors, we analyze the site "representativeness" using the 500m MODIS Land Cover product (MCD12Q1 v6) in 2017, IGBP dataset. First, we take the land cover (LC) type of the MODIS grid cell where a given in-situ site is located as the ground-based LC type. Next, we search all the MODIS grid cells that fall within the SMAP 9km EASE grid cell where this in-situ site is located. The latter area consists of about 20 x 20 = 400 MODIS grid cells. We calculate the fraction of these 400 MODIS grid cells that have the same LC type as the ground-based LC and define this fraction as the site representativeness. We find that 52% of the 2474 sites have site representativeness higher than 50%. When we use only these sites for the RF attribute analysis, the top three factors controlling skill improvement ($R_{L4} - R_{OL}$), L4 skill (R_{L4}), and OL skill (R_{OL}) are still the same, although the precipitation error becomes the top influencer for R_{L4} (not shown).

372

373
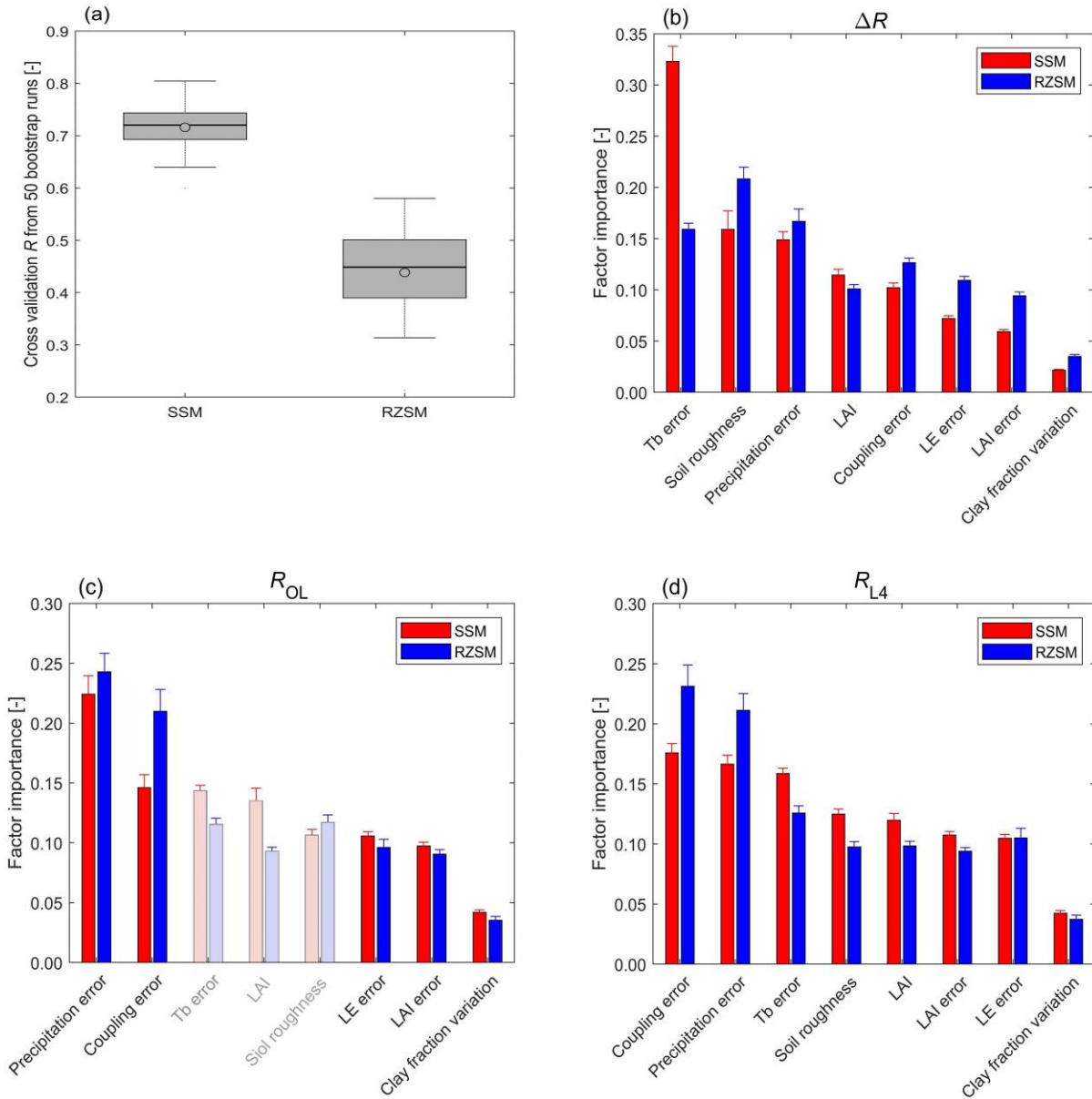
Figure 4: Attribution analysis of SMAP L4 DA skill improvement: (a) Cross-validation of RF regression method in predicting DA skill improvement $\Delta R = R_{L4} - R_{OL}$ based on our eight control factors (Table 1). Relative importance of eight control factors determining spatial patterns in (b) DA skill improvement (ΔR), (c) OL performance (R_{OL}), and (d) L4 performance (R_{L4}). Red (blue) bars represent predictor importance for SSM (RZSM). Error bars reflect the standard deviation from 50-member bootstrapping of the RF importance estimates.

Based on the RF results, the Tb error is quantified as the most prominent factor in determining DA skill improvement (i.e., $\Delta R = R_{L4} - R_{OL}$) – followed by precipitation error and microwave soil roughness (Fig. 4b). The RF-derived ranking of control-factor importance for RZSM is similar to that of SSM in that the same three factors are still the most explanatory. However, relative to SSM, the importance of Tb error for RZSM decreased dramatically from >30% to

17

385 ~15%. Other modeling error sources (e.g., the vertical variability of soil properties) have only very limited impacts on
386 SMAP DA improvement.

387 As seen in Fig. 4c, for the OL performance (R_{OL}), the most important factors identified by RF include precipitation
388 error, SSM-RZSM coupling error, and Tb error (microwave soil roughness) for SSM (RZSM). Note that although the
389 Tb error is identified as third-most important factor for R_{OL} in SSM skill, this is an instance where correlation (i.e.,
390 poorer skill happens to coincide with higher Tb error) does not imply a causal relationship. Specifically, it is expected
391 that Tb (O-F) errors are higher in areas where the OL performs worse, but a high Tb error is not the cause of a low OL
392 performance. The same argument applies to the relationship between microwave soil roughness and OL skill for RZSM
393 estimation. To retain the consistency with analysis of R_{L4} and avoid the misconnection between RTM-related factors
394 and R_{OL}, the bars representing the importance of RTM-related factors to R_{OL} are set semi-transparent in Fig. 3c. The
395 SMAP L4 system is able to reduce impact of precipitation errors on both SSM and RZSM estimation skill, rendering
396 SSM-RZSM coupling error the most important factor for R_{L4} (Fig. 4d). In addition, in the L4 system, the high
397 vegetation density effect on SSM and RZSM estimation is clearly reduced, as the fourth-most important factor of LAI
398 magnitude is replaced by Tb error.

399 The qualitative rankings provided by the RF analysis in Fig. 4 are relatively robust to our particular choice of the
400 benchmark data set to define the 'error' of various control variables. For instance, we replace the CGDPA precipitation
401 benchmark with the Climate Prediction Center Morphing (CMORPH) merged product (Version 1, last access: 6 April
402 2020; DOI: https://doi.org/10.25921/w9va-q159; Xie et al., 2019), which is the 0.1 degree merging product of
403 CMORPH and observations from more than 30,000 automatic weather stations in mainland China. In this case, the
404 predictive power of the regression model established by the RF is not affected (similar to Fig. 4a), and the qualitative
405 rankings of the precipitation error in R_{OL} and R_{L4} are not impacted (similar to Fig. 4c-d).

3.3.2 Attribution using box plot comparisons

407 As stated in Section 2.5, the RF method is adept at summarizing the impact of multiple (co-varying) control factors
408 simultaneously in the established regression model, and thus provides more comprehensive insights than the
409 examination of how the target variable (DA improvement) fluctuates with each individual control factor. However, it
410 does not allow the investigation of the sign of the relationship between DA improvement and each control factor –
411 which is important for understanding how each factor influences the DA system. In addition, since the net impact of
412 various factors can enhance DA skill improvement by either degrading the OL or enhancing the ability of DA to add
413 more value, it is important to decompose the source of variations in ΔR. Therefore, in addition to examining how
414 SMAP DA skill improvement, i.e., $\Delta R = R_{L4} - R_{OL}$, varies as a function of the most prominent control factors identified
415 above in Section 3.3.1 (i.e., Tb error, precipitation forcing error, and microwave soil roughness). We also examine
416 how precipitation error as a control factor affects the OL performance, i.e., R_{OL}.

417 To minimize the uncertainty caused by large errors in each of the control factors, we exclude samples with errors
418 (separately for each control factor) ranking above the 80th percentile in the following analysis. The relationship
419 between Tb errors and L4 DA skill improvement is straightforward: higher Tb errors are associated with higher ΔR,
420 with ΔR generally larger for SSM than for RZSM (Fig. 5a-b).

421
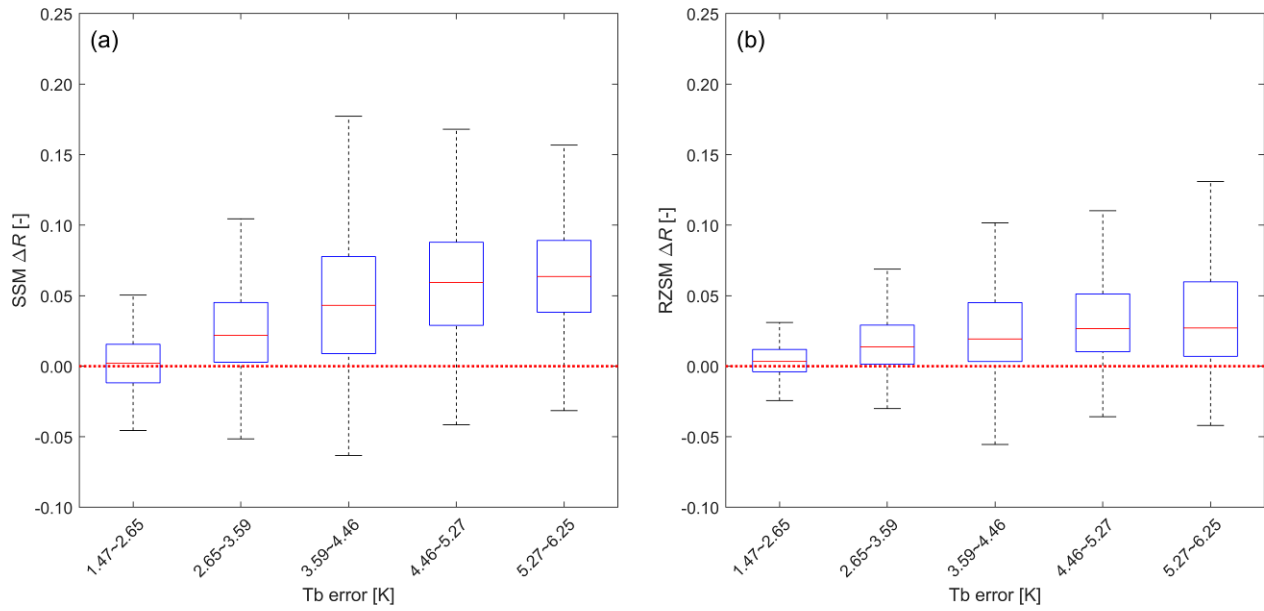
Figure 5: SMAP L4 DA skill improvement ($\Delta R = R_{L4} - R_{OL}$) as a function of Tb error for (a) SSM and (b) RZSM. Samples with Tb error ranking above the 80th percentile are excluded from the analysis.

For precipitation, this decomposition is illustrated in Fig. 6. Note that, as expected, low-quality precipitation tends to degrade the skill (i.e., correlation versus ground observations) of OL SSM and RZSM estimates (see Fig. 6a-b). This degradation provides an enhanced opportunity for SMAP L4 DA to provide benefit. As a result, ΔR tends to be a proportional function of precipitation skill (i.e., higher precipitation skill leads to lower ΔR, see Fig. 6c-d). This inverse relationship is a well-known tendency for land data assimilation systems (Liu et al., 2011; Bolten and Crow, 2012; Dong et al., 2019a). Precipitation quality has a diminished impact on RZSM estimation skill compared to SSM estimation skill. This is expected since RZSM is (essentially) the result of applying a low-pass time series filter to precipitation. As such, it is less sensitive to high-frequency errors in precipitation products than SSM is.

433

434
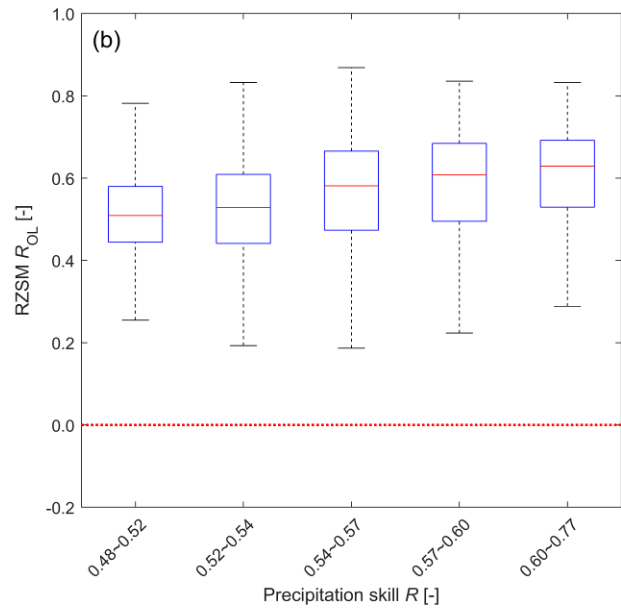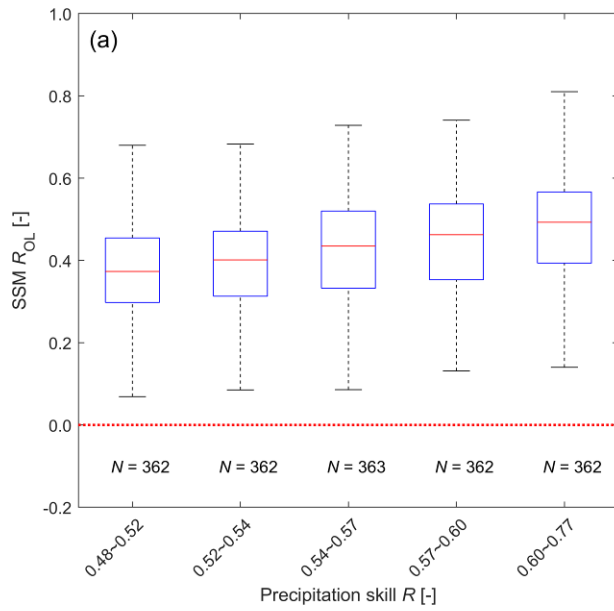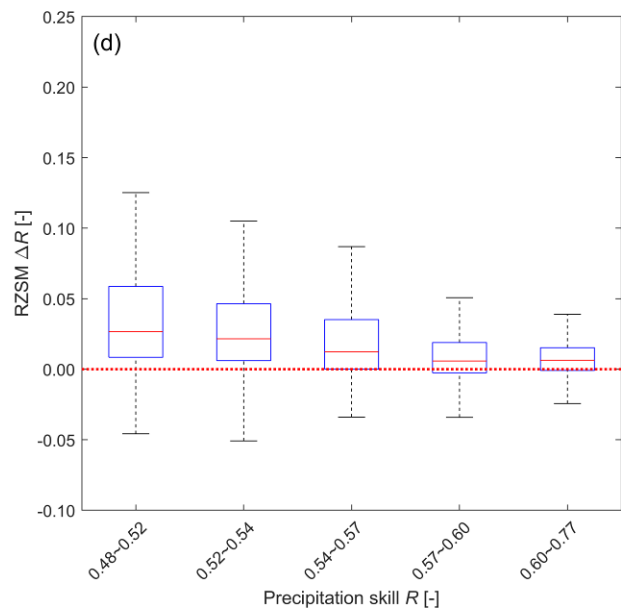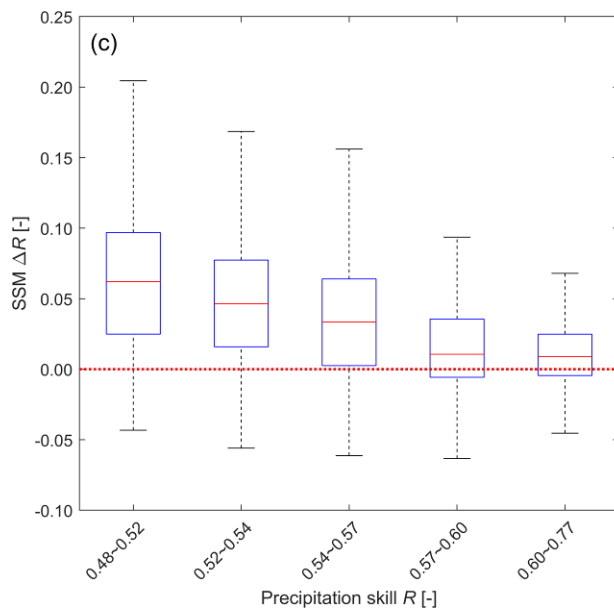
Figure 6: OL performance (R_{OL}) as a function of precipitation forcing skill R for (a) SSM and (b) RZSM. SMAP L4 DA skill improvement ($\Delta R = R_{\text{L4}} - R_{\text{OL}}$) as a function of precipitation skill for (c) SSM and (d) RZSM. Samples with precipitation skill ranking below the 20th percentile are excluded from the analysis.

Figure 7 is analogous to Fig. 5 but shows skill differences ΔR as a function of microwave soil roughness. Similar to Tb errors, it is as expected that this control factor of microwave soil roughness has little impact on the OL performance, except that R_{OL} shows slight decreasing tendency with increasing soil roughness (not shown). Given the fact that the

20

442   OL does get worse with increasing roughness, there is more room for improvement in areas with higher soil roughness,

443   which makes it plausible that ΔR increases with increasing soil roughness (see Fig. 7a-b).

444
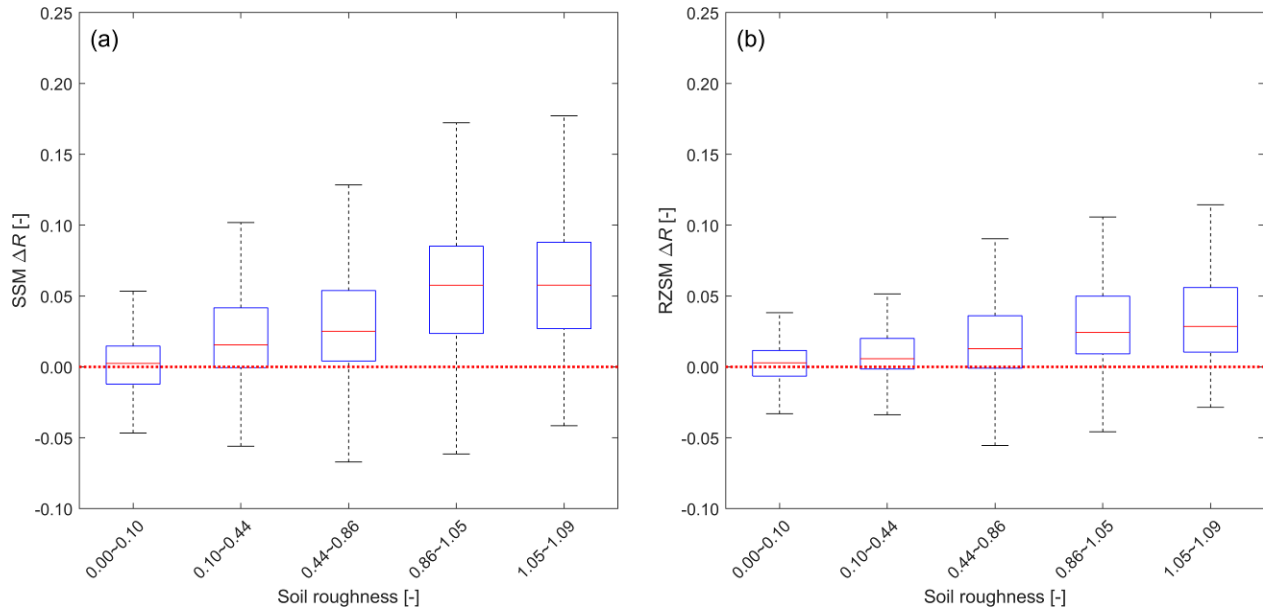
Figure 7: As in Fig. 5 but for ΔR as a function of microwave soil roughness.

446

447   Besides the above three control factors that dominate the DA skill improvement, we also examine the top factor that

448   affects SMAP L4 performance, i.e., vertical-coupling errors (Fig. 8). As expected, larger (absolute) bias in SSM-RZSM

449   coupling in CLSM tends to be associated with degraded OL estimates of both SSM and RZSM (see Figs. 8a-b),

450   although the analysis does not prove such a causal relationship. Similar to precipitation errors above, decreased OL

451   skill (seen on the left-hand-side of the figures) provides an opportunity for increased DA skill improvement – which

452   is clearly seen in Fig. 8. However, such increases are much larger for SSM than for RZSM.

453   For RZSM, SSM-RZSM coupling bias exerts both positive and negative effects on estimation accuracy. While such

454   bias leads to an enhanced opportunity to improve upon a degraded OL, it should also hamper the ability of DA to

455   transfer SSM increments into the root-zone – particularly when, like here, the bias reflects the lack of vertical coupling

456   in the model (Kumar et al., 2009). This means that some of the opportunity presented by the larger RZSM errors in

457   OL is squandered by sub-optimal DA. As a result, the increase in RZSM DA skill improvement associated with biased

458   SSM-RZSM coupling (Fig. 8d) is smaller than the analogous increase in SSM DA skill improvement (Fig. 8c).

459

460
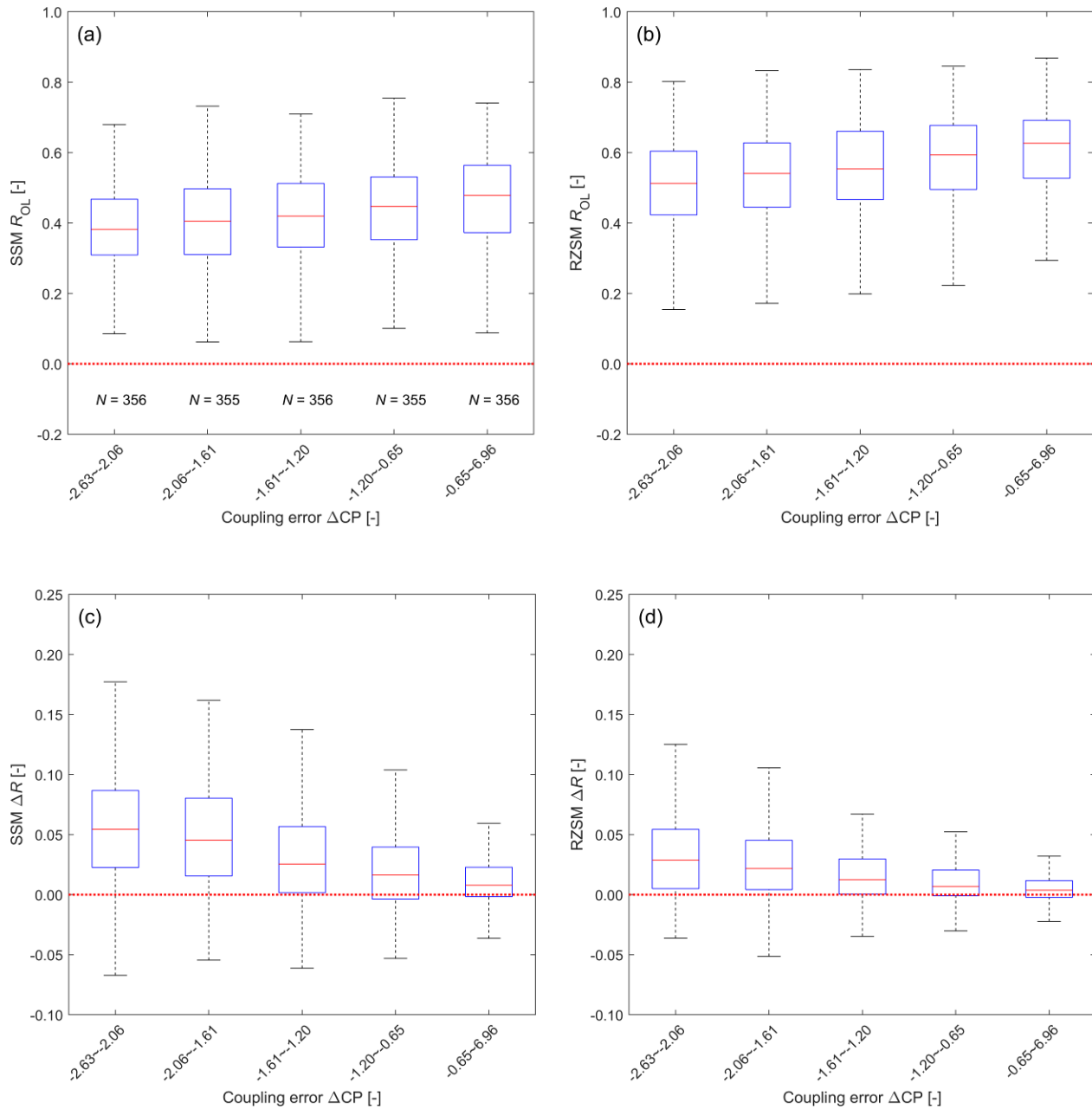
Figure 8: As in Fig. 6 but for R_{OL} and ΔR as a function of SSM-RZSM coupling error indicated by the CP difference (ΔCP = CP_{OL} - CP_{obs}).

For the three strongest control factors that determine DA skill improvement ΔR, i.e., Tb error, precipitation error and microwave soil roughness, we further conducted paired one-way analysis of variance. Results indicates that for each of the five binned groups separated by each of the above-mentioned three control factors, the inter-group difference in ΔR caused by each control factor is significant ($p<0.01$) for both SSM and RZSM. In addition, except for the groups with lowest mean ΔR in Fig. 5a and Fig. 7a, the averages of ΔR from all groups are significantly higher than 0 ($p<0.01$).

22

4 Conclusions

The SMAP L4 algorithm assimilates L-band Tb observations into the Catchment Land Surface Model to provide surface and root-zone soil moisture estimates (i.e., SSM, RZSM) with global, 3-hourly coverage at 9-km resolution. The performance of the L4 soil moisture estimates compared to a baseline model-only simulation (OL) is influenced by multiple control factors associated with CLSM and the tau-omega RTM components of the L4 system. In this study, we assess the performance of SMAP L4 DA system using two years of in-situ soil moisture profile observations at 2474 sites across mainland China. We apply a random forest (RF) regression to identify the dominant factors (from a pre-defined list) that control the spatial distribution of the DA skill improvement (defined as the skill difference between the L4 and OL estimates of SSM and RZSM as measured by their Spearman rank correlation with in-situ measurements). Results show that L4 improves SSM prediction skill by 14% on average, with over 77% of the 2287 9-km EASE grid cells showing an increase in Spearman's rank correlation with in-situ observations. Similarly, widespread, though smaller, improvements are observed in RZSM, with averaged R improvement of 7%.

Based on the RF regression analysis, the benefit of SMAP L4 DA for SSM is primarily determined by Tb error (measured by standard deviation of O-F Tb residuals), followed by microwave soil roughness and daily precipitation error. These three factors are also the most prominent factors controlling SMAP DA improvement for RZSM, albeit with the Tb error being the least important of these three factors for RZSM DA skill improvement.

Generally, the OL performance clearly decreases with increasing precipitation error, whereas for L4 performance precipitation error is not identified as the most dominant control factor. This indicates that the L4 system is able to correct for errors in precipitation forcing. In addition, our results demonstrate that SMAP DA contributes the most benefit for cases where CLSM underestimates SSM-RZSM vertical coupling strength. However, due to the difference in top-layer soil depth between the in-situ observations (10 cm) and the L4 analysis (5 cm), it is unclear whether or not the observed SSM-RZSM coupling strength biases are real in an absolute sense – or simply reflect inconsistencies in the depth of modelled versus observed SSM and RZSM time series. Nevertheless, it is worth stressing that, despite the ambiguity about their absolute magnitude/sign, relative variations in apparent SSM-RZSM coupling biases explain a significant amount of the observed spatial variation in L4 performance. Therefore, this finding clearly underpins the importance of properly specifying SSM-RZSM coupling strength in CLSM as a way to improve the SMAP L4 product. For SMAP L4 SSM skill, the next-most important factors (after SSM-RZSM coupling) are the precipitation error, the Tb error and microwave soil roughness (Fig. 4d). For L4 RZSM skill, the next-most important factors (after SSM-RZSM coupling) are the precipitation error, the Tb error and the LE error, with the latter two factors of comparable importance (Fig. 4d). To enhance the L4 performance, additional focus should thus be placed on improving the model's characterization of the microwave radiative transfer modeling (Tb error), together with the partitioning of the available energy into latent and sensible heat (LE error).

Some of our RF analysis results fall squarely within expectation; for instance, the OL skill is predominately determined by precipitation error, and L4 skill improvement (i.e., R_{L4} - R_{OL}) is mostly determined by Tb error. On the other hand, there are also some more surprising results. For instance, we found that SSM-RZSM coupling error and precipitation error have a comparable impact on OL. For L4 skill, however, the impact of SSM-RZSM coupling error exceeds that of precipitation error. More specifically, L4 DA contributes the most benefit for cases where CLSM underestimates

506 SSM-RZSM vertical coupling strength. These findings could be used for L4 product development. In addition, this
507 study pinpoints that the L4 skill improvement is not heavily impacted by LAI magnitude, which gives confidence for
508 using the L4 product over densely vegetated areas.

509 **Data availability**

510 The SMAP L4 datasets are available from https://nsidc.org/data/SPL4SMAU/versions/4. Gauge-based precipitation
511 dataset CGDPA is from http://data.cma.cn/data/cdcdetail/dataCode/SEVP_CLI_CHN_PRE_DAY_GRID_0.25.html.
512 The availabilities of other datasets are stated in their corresponding subsections.

513 **Author contributions**

514 Jianxiu Qiu and Jianzhi Dong conceptualized the study. Jianxiu Qiu carried out the analysis and wrote the first draft
515 manuscript, Wade Crow refined the work, Jianzhi Dong, Rolf Reichle, and Gabrielle De Lannoy helped with the
516 analysis. All authors contributed to the analysis, interpretation of the results and writing.

517 **Competing interests**

518 The authors declare that they have no conflict of interest.

524 **References**

525 Baret, F., Weiss, M., Lacaze, R., Camacho, F., Makhmara, H., Pacholcyzk, P., and Smets, B.: GEOV1: LAI, FAPAR
526 Essential Climate Variables and FCOVER global time series capitalizing over existing products. Part1: Principles of
527 development and production, Remote Sens. Environ., 137, 299-309, doi:10.1016/j.rse.2013.02.030, 2013.

528

529 Bolten, J.D. and Crow, W.T.,: Improved prediction of quasi-global vegetation conditions using remotely-sensed
530 surface soil moisture, Geophys. Res. Lett., 39(19), doi:10.1029/2012GL053470, 2012.

531

532 Breiman, L.: Random forests, Mach. Learn., 45(1), 5–32, doi:10.1023/A:1010933404324, 2001.

533

534 Chan, S., Njoku, E. G. and Colliander A.: SMAP L1C radiometer half-orbit 36 km EASE-Grid brightness temperatures,

535 version 3. NASA National Snow and Ice Data Center Distributed Active Archive Center, 10.5067/E51BSP6V3KP7,

536 2016.

537

538 Chen, F., Crow, W.T., Starks, P.J. and Moriasi, D.N.: Improving hydrologic predictions of a catchment model via

539 assimilation of surface soil moisture, Adv. Water Resources., 34(4), 526-536, doi:10.1016/j.advwatres.2011.01.011,

540 2011.

541

542 Chen, F., Crow, W.T., Colliander, A., Cosh, M.H., Jackson, T.J., Bindlish, R., Reichle, R.H., Chan, S.K., Bosch, D.D.,

543 Starks, P.J., and Goodrich, D.C.: Application of triple collocation in ground-based validation of Soil Moisture

544 Active/Passive (SMAP) level 2 data products, IEEE JSTARS., 99, 1-14, doi:10.1109/JSTARS.2016.2569998, 2016.

545

546 Crow, W.T. and Van Loon, E.: The impact of incorrect model error assumptions on the sequential assimilation of

547 remotely sensed surface soil moisture, J. Hydrometeorol., 8(3), 421-431, doi:10.1175/jhm499.1, 2006.

548

549 De Lannoy, G. J. M., Reichle, R. H., and Pauwels, V. R. N.: Global calibration of the GEOS-5 L-band microwave

550 radiative transfer model over nonfrozen land using SMOS observations, J. Hydrometeorol., 14(3), 765–785,

551 doi:10.1175/JHM-D-12-092.1, 2013.

552

553 De Lannoy, G. J. M., Reichle, R. H., and Vrugt, J. A.: Uncertainty quantification of GEOS-5 L-band radiative transfer

554 model parameters using Bayesian inference and SMOS observations, Remote Sens. Environ., 148, 146–157,

555 doi :10.1016/j.rse.2014.03.030, 2014.

556

557 Dong, J., Crow, W.T., Reichle, R., Liu, Q., Lei, F., and Cosh, M.: A global assessment of added value in the SMAP

558 Level 4 soil moisture product relative to its baseline land surface model, Geophys. Res. Lett., 46, 6604-6613,

559 doi:10.1029/2019GL083398, 2019a.

560

561 Dong, J., Crow, W.T., Duan, Z., Wei, L., and Lu, Y.: A double instrumental variable method for geophysical product

562 error estimation, Remote Sens. Environ., 225, 217-228, doi:10.1016/j.rse.2019.03.003, 2019b.

563

564 Dong, J., Crow, W.T., Tobin, J. K., Cosh, H. M., Bosch, D. D., Starks, J. P., Seyfried, M., and Collins, H. C.:

565 Comparison of microwave remote sensing and land surface modeling in surface soil moisture climatology estimation,

566 Remote Sens. Environ., 242, 111756, doi :10.1016/j.rse.2020.111756, 2020.

567

568 Entekhabi, D., Njoku, E. G., O'Neill, P. E., Kellogg, K. H., Crow, W. T., and Edelstein, W. N.: The soil moisture active

569 passive (SMAP) mission, P. IEEE., 98(5), 704–716, doi:10.1109/jproc.2010.2043918, 2010.

570

571 FAO/IIASA/ISRIC/ISSCAS/JRC (2012), Harmonized World Soil Database (version 1.2), Food and Agric. Organ.,

572 Rome. Available at: http://webarchive.iiasa.ac.at/Research/LUC/External-World-soil-database/HTML.

573

574 Gupta, H. V., Kling, H., Yilmaz, K. K., and Martinez, G. F.: Decomposition of the mean squared error and NSE

575 performance criteria: Implications for improving hydrological modelling, J. Hydrometeorol., 377(1-2), 80-91,

576 doi:10.1016/j.jhydrol.2009.08.003, 2009.

577

578 Han, S., Shi, C. X., Jiang, L. P., Zhang, T., Liang, X., Jiang, Z. W., Xu, B., Li, X. F., Zhu, Z., Lin, H. J.: The simulation

579 and evaluation of soil moisture based on CLDAS, J. Applied Meteorol. Sci., 28(3), 369-378, doi:10.11898/1001-

580 7313.20170310, 2017.

581

582 Jung, M., Koirala, S., Weber, U., Ichii, K., Gans, F., Camps-Valls, G., and Reichstein, M.: The FLUXCOM ensemble

583 of global land-atmosphere energy fluxes, Sci. Data., 6(1), 1-14, doi:10.1038/s41597-019-0076-8, 2019.

584

585 Kumar, S.V., Reichle, R.H., Koster, R.D., Crow, W.T., and Peters-Lidard, C.D.: Role of subsurface physics in the

586 assimilation of surface soil moisture observations, J. Hydrometeorol., 10, 1534-1547, doi:10.1175/2009JHM1134.1,

587 2009.

588

589 Lucchesi, R.: File specification for GEOS-5 FP, NASA GMAO Office Note 4 (version 1.0), 63 pp. Available at

590 https://ntrs.nasa.gov, 2013.

591

592 Mahanama, S. P., Koster R. D., Walker G. K., Takacs L. L., Reichle R. H., De Lannoy G., Liu Q., Zhao B., and Suarez

593 M. J.: Land boundary conditions for the Goddard Earth Observing System model version 5 (GEOS-5) climate modeling

594 system–Recent updates and data file descriptions. NASA/TM-2015-104606, Vol. 39, 55 pp. NASA Goddard Space

595 Flight Center, Greenbelt, MD. Available at https://ntrs.nasa.gov/search.jsp?R=20160002967, 2015.

596

597 McColl, K., Vogelzang, J., Konings, A.G., Entekhabi, D., Piles, M., and Stoffelen, A.: Extended triple collocation:

598 Estimating errors and correlation coefficients with respect to an unknown target, Geophys. Res. Lett., 41(17), 6229-

599 6236, doi:10.1002/2014gl061322, 2014.

600

601 Piepmeier, J. R., Focardi, P., Horgan, K. A., Knuble, J., Ehsan, N., Lucey, J., Brambora, C., Brown, P. R., Hoffman,

602 P. J., French, R. T., Mikhaylov, R. L., Kwack, E. Y., Slimko, E. M., Dawson, D. E., Hudson, D., Peng, J., Mohammed,

603 P. N., de Amici, G., Freedman, A. P., Medeiros, J., Sacks, F., Estep, R., Spencer, M. W., Chen, C. W., Wheeler, K. B.,

604 Edelstein, W. N., O'Neill, P. E., and Njoku, E. G.: SMAP L-band microwave radiometer: Instrument design and first

605 year on orbit, IEEE T. Geosci. Remote., 55(4), 1954–1966, doi:10.1109/TGRS.2016.2631978, 2017.

606

607   Liu, Q., Reichle, R., Bindlish, R., Cosh, M.H., Crow, W.T., de Jeu, R., de Lannoy, G., Huffman, G.J. and Jackson,
608   T.J.: The contributions of precipitation and soil moisture observations to the skill of soil moisture estimates in a land
609   data assimilation system, J. Hydrometeorol., 12(5), 750-765, doi:10.1175/JHM-D-10-05000.1, 2011.
610
611   Reichle, R.H., Crow, W.T., Koster, R. D., Sharif, H. and Mahanama, S.: Contribution of soil moisture retrievals to
612   land data assimilation products, Geophys. Res. Lett., 35(1), doi:10.1029/2007GL031986, 2008.
613
614   Reichle, R. H., de Lannoy, G. J. M., Liu, Q., Ardizzone, J. V., Colliander, A., Conaty, A., Crow, W., Jackson, T. J.,
615   Jones, L. A., Kimball, J. S., Koster, R. D., Mahanama, S. P., Smith, E. B., Berg, A., Bircher, S., Bosch, D., Caldwell,
616   T. G., Cosh, M., González-Zamora, Á., Holifield Collins, C. D., Jensen, K. H., Livingston, S., Lopez-Baeza, E.,
617   Martínez-Fernández, J., McNairn, H., Moghaddam, M., Pacheco, A., Pellarin, T., Prueger, J., Rowlandson, T., Seyfried,
618   M., Starks, P., Su, Z., Thibeault, M., van der Velde, R., Walker, J., Wu, X., and Zeng, Y.: Assessment of the SMAP
619   Level-4 surface and root-zone soil moisture product using in situ measurements, J. Hydrometeorol., 18(10), 2621–
620   2645, doi:10.1175/JHM-D-17-0063.1, 2017a.
621
622   Reichle, R. H., de Lannoy, G. J. M., Liu, Q., Koster, R. D., Kimball, J. S., Crow, W. T., Ardizzone, J. V., Chakraborty,
623   P., Collins, D. W., Conaty, A. L., Girotto, M., Jones, L. A., Kolassa, J., Lievens, H., Lucchesi, R. A., and Smith, E. B.:
624   Global assessment of the SMAP Level-4 surface and root-zone soil moisture product using assimilation diagnostics, J.
625   Hydrometeorol., 18(12), 3217–3237, doi:10.1175/jhm-d-17-0130.1, 2017b.
626
627   Reichle, R. H., de Lannoy, G., Koster, R. D., Crow, W. T., Kimball, J. S., and Liu, Q.: SMAP L4 Global 9 km EASE-
628   grid surface and root zone soil moisture land model constants, Version 4, NASA National Snow and Ice Data Center
629   DAAC, https://doi.org/10.5067/KGLC3UH4TMAQ, 2018a.
630
631   Reichle, R. H., de Lannoy, G., Koster, R. D., Crow, W. T., Kimball, J. S., & Liu, Q.: SMAP L4 global 3-hourly 9 km
632   EASE-grid surface and root zone soil moisture analysis update data, version 4, NASA National Snow and Ice Data
633   Center DAAC, https://doi.org/10.5067/60HB8VIP2T8W, 2018b.
634
635   Reichle, R. H., de Lannoy, G., Koster, R. D., Crow, W. T., Kimball, J. S., & Liu, Q.: SMAP L4 global 3-hourly 9 km
636   EASE-grid surface and root zone soil moisture geophysical data, version 4, NASA National Snow and Ice Data Center
637   DAAC, https://doi.org/10.5067/KPJNN2GI1DQR, 2018c.
638
639   Reichle, R. H., Liu, Q., Koster, R. D., Crow, W. T., De Lannoy, G. J., Kimball, J. S., and Kolassa, J.: Version 4 of the
640   SMAP Level-4 soil moisture algorithm and data product, J. Adv. Model Earth Sy., 11(10), 3106-3130,
641   doi:10.1029/2019MS001729, 2019.
642

643   Reichle, R. H., and Coauthors (2020), The contributions of gauge-based precipitation and SMAP brightness

644   temperature observations to the skill of the SMAP Level-4 soil moisture product, J. Hydrometeorol., accepted,

645   doi:10.1175/JHM-D-20-0217.1.

646

647   Seneviratne, S. I., Corti, T., Davin, E. L., Hirschi, M., Jaeger, E. B., and Lehner, I.: Investigating soil moisture–climate

648   interactions in a changing climate: A review, Earth-Sci. Rev., 99, 125–161, doi:10.1016/j.earscirev.2010.02.004, 2010.

649

650   Seneviratne, S. I., Wilhelm, M., Stanelle, T., Hurk, B., Hagemann, S., and Berg, A.: Impact of soil moisture-climate

651   feedbacks on CMIP5 projections: First results from the GLACECMIP5 experiment, Geophys. Res. Lett., 40(19), 5212-

652   5217, doi:10.1002/grl.50956, 2013.

653

654   Shen, Y., Xiong, A., Wang, Y., and Xie, P.: Performance of high-resolution satellite precipitation products over China,

655   J. Geophys. Res-Atmos., 115(D2), doi:10.1029/2009JD012097, 2010.

656

657   Shen, Y. and Xiong, A.: Validation and comparison of a new gauge-based precipitation analysis over mainland China,

658   Int. J. Climatol., 36(1), 252-265, doi:10.1002/JOC.4341, 2015.

659

660   Verger, A., Baret, F., and Weiss, M.: Performances of neural networks for deriving LAI estimates from existing

661   CYCLOPES and MODIS products, Remote Sens. Environ., 112, 2789-2803, doi:10.1016/j.rse.2008.01.006, 2008.

662

663   Xie, P., Yatagai, A., Chen, M., Hayasaka, T., Fukushima, Y., Liu, C., and Yang, S.: A gauge-based analysis of daily

664   precipitation over East Asia, J. Hydrometeorol., 8, 607-626, doi:10.1175/JHM583.1, 2007.

665

666   Xie, P., Joyce, R., Wu, S., Yoo, S.-H., Yarosh, Y., Sun, F., Lin, R..: NOAA CDR Program: NOAA Climate Data

667   Record (CDR) of CPC Morphing Technique (CMORPH) High Resolution Global Precipitation Estimates, Version 1.

668   NOAA National Centers for Environmental Information, 2019.

669